Materials Science & Engineering A 773 (2020) 138840

Contents lists available at ScienceDirect

Materials Science & Engineering A

journal homepage: http://www.elsevier.com/locate/msea

Microstructure and mechanical properties of (B_4C+Al_2O_3)/Al composites designed for neutron absorbing materials with both structural and functional usages

Y.N. Zan [a,c,1], Y.T. Zhou [a,1], Z.Y. Liu [a], Q.Z. Wang [b,**], W.G. Wang [a], D. Wang [a], B.L. Xiao [a], Z. Y. Ma [a,*]

[a] Shenyang National Laboratory for Materials Science, Institute of Metal Research, Chinese Academy of Sciences, 72 Wenhua Road, Shenyang, 110016, China
[b] Key Laboratory of Nuclear Materials and Safety Assessment, Institute of Metal Research, Chinese Academy of Sciences, 72 Wenhua Road, Shenyang, 110016, China
[c] School of Materials Science and Engineering, University of Science and Technology of China, 72 Wenhua Road, Shenyang, 110016, China

ARTICLE INFO

Keywords:
Metal-matrix composites
Neutron absorbing materials
Microstructure
Mechanical properties
High-temperature strength

ABSTRACT

To meet the demand for the new generation of neutron absorber materials (NAMs) for the dry storage of the spent nuclear fuels, (B_4C + Al_2O_3)/Al composites were fabricated by powder metallurgy technique using ultrafine Al powders. The composites designed with various fabricating parameters and fabricated at various sintering temperatures were characterized by electron microscopy and mechanically tested. The sample sintered at 450 °C shows the best strength-ductility balance at 350 °C (106.2 MPa in ultimate tensile strength and 9.6% in elongation). Addition of B_4C particles and increase of the Al_2O_3 film thickness could enhance the strength of the composites at room temperature but showed no obvious effect on the strength at 350 °C. When sintering temperature of the composites increased from 450 °C to 550 °C, the transformation of amorphous Al_2O_3 lamellae to γ-Al_2O_3 particles led to deterioration of the strength of the composites. Based on the analyses of both high-temperature deformation mechanism and strengthening mechanism, it was considered that the amorphous Al_2O_3 could pin the grain boundaries and prevent them from gliding, which was the main factor to significantly increase the high-temperature strength. Based on the results, a strategy to design the aluminium matrix NAMs with excellent high-temperature strength was proposed.

1. Introduction

The development of nuclear power results in increased amount of spent nuclear fuels. Neutron absorber materials (NAMs) are necessary for the transportation and the storage of spent nuclear fuels [1–4]. Aluminium matrix composites (AMCs) containing B_4C particles are increasingly used in the nuclear industry because of the large neutron absorption cross-section of ^{10}B in B_4C.

So far, most of the studies of B_4C/Al NAMs are focused on conventional B_4C/6xxx or B_4C/1xxx composites for the wet storage of the spent nuclear fuels [1,5–9]. Over the years, the novel dry storage method is replacing the wet storage gradually for its safety and economy. However, since the strength of these composites under actual service environment of NAMs (up to 350 °C) [8] is not enough for bearing load, they can only serve as functional materials (neutron absorbing). Extra structural materials must be used together for load bearing. In consideration of heat transfer and weight reduction, which is of great significance for dry storage, developing the B_4C/Al composites which are strong enough for structural usage is extremely meaningful.

Traditional precipitation-strengthened high strength aluminium alloys (such as 2xxx and 7xxx series) usually have poor high-temperature strength [10]. Even for aluminium alloys designed for high-temperature application (such as Al–Si–Cu and Al–Si–Mg alloys) [11,12], they could hardly serve at above 300 °C for long-term application because of precipitate coarsening; so research was mainly focused on the instantaneous strength [13–15].

Sintered Al powders (SAPs) developed in 1950s provides an inspiration to fabricate AMCs for long-term service under high temperature

* Corresponding author.
** Corresponding author.
E-mail address: zyma@imr.ac.cn (Z.Y. Ma).
[1] These authors contributed equally to this work.

https://doi.org/10.1016/j.msea.2019.138840
Received 18 September 2019; Received in revised form 17 December 2019; Accepted 17 December 2019
Available online 19 December 2019
0921-5093/

[16,17]. Al_2O_3 formed on Al powder surface during ball-milling process could enhance high-temperature strength significantly. However, the ball-milling process is time consuming and vulnerable to risks. Furthermore, recent reports revealed that SAPs usually exhibited limited ductility at room temperature (RT) [18], which make them incompetent for practical application. This is because the ultrafine grains generated during ball-milling usually exhibited poor strain hardening capability, resulting in the poor ductility of SAPs.

An alternative method for introducing Al_2O_3 is to adopt ultrafine Al powders for powder metallurgy processing. Poletti et al. [10] studied the high-temperature strength of Al_2O_3/Al composites compacted from aluminium powders with a mean diameter of 700 nm and reported that the compressive strength could be over 150 MPa at 400 °C with ductility being still preserved. This indicates that adopting ultrafine Al powders might be one possible way to fabricate the desired NAMs for both structural and functional usages. However, such NAMs have not been reported so far to the best of our knowledge. The effect of B_4C addition on the mechanical properties of the Al_2O_3/Al composites stays unclear, which represents a crucial issue in the engineering application for such NAMs. Furthermore, since the thickness of oxidation film of ultrafine Al powders could be increased by pre-oxidation, figuring out whether the strength of the composites can be enhanced by thicker Al_2O_3 film is also of great significance.

In previous studies on the Al_2O_3/Al composites compacted from aluminium powders, it was found that high-temperature strength could be enhanced by preventing the amorphous Al_2O_3 (am-Al_2O_3) from transforming into γ-Al_2O_3 [19]. Understanding the strengthening mechanisms relevant to the strength enhancement will be very meaningful for directing the design of high-temperature materials. According to the theory of strengthening mechanisms, the strengthening effects by load-transfer and grain boundary (GB) pinning of Al_2O_3 which was located at the GBs should both be responsible for high-temperature strengthening in the Al_2O_3/Al composites, however, which mechanism is the main factor stays unclear.

In this study, ($B_4C + Al_2O_3$)/Al NAMs were fabricated using ultrafine Al powders, and the influences of Al_2O_3 and B_4C particles on the mechanical properties were studied. The aims of this study are (a) to develop new NAMs with excellent strength-ductility balance for dry storage, (b) to elucidate the strengthening mechanisms as well as the deformation mechanism at high temperature and (c) to identify the dominant factor to enhance the high-temperature strength of the composites.

2. Experimental procedure

Pure Al powders and B_4C particles with the mean sizes of 1.45 μm and 6.5 μm were used as the matrix and reinforcement, respectively (shown in Fig. 1). Four different composites were fabricated by powder metallurgy (PM) technique using ultrafine Al powders, and specific fabrication processes are summarized in Table 1.

For Composite I, ultrafine Al powders were used without pre-oxidation and B_4C particle addition. For composites II and IV, 10.0 wt % (10.6 vol%) B_4C particles were mixed into ultrafine Al powders. For Composite III, ultrafine Al powders were pre-oxidized and then mixed with 10.0 wt% B_4C particles. The pre-oxidation of Al powders was carried out at 400 °C for 2 h in the furnace with air atmosphere to increase the thickness of the oxidation film. The mixing of the Al powders and B_4C particles was performed in a bi-axis rotary mixer for 8 h with a rotation speed of 50 rpm and a ball-to-powder ratio of 1:1.

Billets with a height of 30 mm and a diameter of 40 mm were produced by hot isostatic pressing (HIP) at 450 °C or 550 °C. Before HIP, vacuum degassing was carried out at 350 °C. For comparison, a conventional 10.0 wt%B_4C/Al composite was fabricated by HIP using coarse Al powders with an average diameter of 13 μm (Composite V). All the composite billets were forged at 450 °C with a reduction ratio of 4:1.

The microstructure of the composites was observed perpendicular to the forging direction using optical microscopy (OM, Zeiss Axiovert 200MAT) and transmission electron microscopy (TEM, FEI Tecnai F30). The specimens for OM were ground and then mechanically polished. Specimens for TEM were prepared by metallographic grinding and dimpling, followed by milling using a Gatan PIPS (Model 695).

Tensile specimens with a gauge length of 5 mm, a width of 1.7 mm and a thickness of 1.2 mm were machined from the forged disks with the axis parallel to the radial direction of the disks. At least 5 tensile specimens were tested for each composite at a strain rate of 1×10^{-3} s^{-1} at both RT and 350 °C using an Instron 5582 tester. To disclose the reason for different high-temperature strengths of Composites II and IV, tensile specimens with a gauge length of 10 mm, a width of 3 mm and a thickness of 2.5 mm were tested at 350 °C with fractured specimens being immediately quenched after testing, and then TEM specimen was sampled near the cracked point and observed. Fractographs were observed using scanning electron microscopy (SEM, Leo Supra 55). Additional tensile tests of Composites II and IV were conducted at strain rates from 1×10^{-4} to 1×10^{-1} s^{-1} at 350 °C to study the deformation mechanism of the composites.

Table 1
Composites fabricated with different compositions and processes.

Composites	Size of Al powders	Pre-oxidation of Al powders	B_4C content	HIP temperature
Composite I	1.45 μm	None	None	450 °C
Composite II	1.45 μm	None	10.0 wt%	450 °C
Composite III	1.45 μm	Yes (400 °C/2 h)	10.0 wt%	450 °C
Composite IV	1.45 μm	None	10.0 wt%	550 °C
Composite V	13 μm	None	10.0 wt%	600 °C

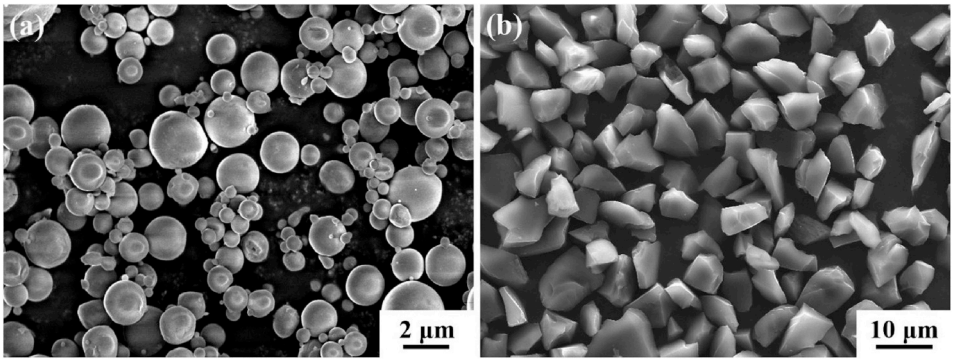

Fig. 1. SEM micrographs showing (a) ultrafine Al powders and (b) B_4C particles.

3. Results

3.1. Microstructure

3.1.1. Distribution of B_4C particles in the composites

Fig. 2 shows the B_4C distribution in Composites II, III and IV. As denoted in Fig. 2a and b, some particle-free zones were observed in Composites II and III, and the distribution of B_4C particles in Composite IV was more homogeneous. This implies that more sufficient material flow happened in Composite IV during forging. The reason will be discussed in the follow-up.

3.1.2. Distribution of Al_2O_3 in the composites

TEM micrographs of various composites are shown in Fig. 3. Lamellar Al_2O_3 was distributed at the grain boundaries of Al matrix in Composites II and III (Fig. 3a and c), which was consistent with previous study [20]. Higher-magnification TEM images shown in Fig. 3b and d indicated that the thickness of single-layer am-Al_2O_3 film increased from 5 nm to 7 nm after pre-oxidation. In Fig. 3d, the original surface between Al and Al_2O_3 can be still distinguished, because the increase of the Al_2O_3 film thickness happened at one side of Al_2O_3, indicating the oxidation process towards the inside of Al powders. Thicker Al_2O_3 layers composed of Al_2O_3 on two adjacent original Al powders could also be found, as shown in the insets of Fig. 3b and d, which were two times as thick as single-layer Al_2O_3. The contents of Al_2O_3 in Composites II and III were calculated to be 2.1 vol% and 2.9 vol%, respectively, by using the average diameter and Al_2O_3 layer thickness of Al powders.

The average length of Al_2O_3 in the two composites was determined to be 260 nm and 310 nm, respectively, by analyzing more than 15 images for each composite. In the deformation process, an Al_2O_3 platelet will be broken when the stress transferred by the Al matrix exceeds the strength of Al_2O_3. The transferred stress is proportional to the length of Al_2O_3, therefore, a critical length exists, and Al_2O_3 with the length less than this critical length cannot be broken. The critical length depends on the strength of Al and Al_2O_3, and the thickness of Al_2O_3 [21]. The thicker the Al_2O_3 is, the harder it is to break during the deformation process. Therefore, the larger length of Al_2O_3 in Composite III was ascribed to its larger thickness.

When HIP was performed at 550 °C, am-Al_2O_3 was found to crystallize during the HIP process. This phenomenon was also reported in previous study [19]. Al_2O_3 in Composite IV exhibited a discontinuous distribution at the Al grain boundaries, as shown in Fig. 3e. The high resolution TEM image in Fig. 3f and the Fast Fourier transform (FFT) shown in the inset confirmed the crystal form as γ-Al_2O_3.

3.1.3. Grain structure of the composites

Grain structure of the composites is shown in Fig. 4. The spherical grains of original powders were deformed into lamellar shape during the forging process. Poletti et al. [10] studied the deformation of Al_2O_3/Al composite fabricated using ultrafine Al powders and discovered that deformation in the temperature range of 350–500 °C at low strain rates did not change the original Al_2O_3/Al grain structure, in which Al_2O_3 was located at the Al grain boundaries. The same grain structure was observed in the present study.

No significant difference in the grain structure was found among Composites I, II and III at this magnification, indicating that the increase in the thickness of Al_2O_3 film and addition of B_4C particles could hardly influence the grain structure of the final composites. However, the grains in Composite IV were found to exhibit larger grain size compared to other composites, although the forging processes were applied at the same ratio. It was reported that both am-Al_2O_3 and γ-Al_2O_3 can prevent the grains from growing when being statically annealed up to 600 °C [19]. Therefore, the difference in the grain size was a result of the thermal-deformation process.

The difference in the grain size can be attributed to the effect of Al_2O_3 on GB pinning. On the one hand, particulate γ-Al_2O_3 would exhibit weaker ability in pinning GBs than lamellar am-Al_2O_3. Consequently, in the forging deformation, the grains would grow up more easily in Composite IV. On the other hand, when a polycrystalline is deformed, there are mainly two kinds of deformation mechanisms: quasi-uniform flow by dislocation glide or dislocation creep and non-uniform flow by grain-boundary sliding [22]. The feature of the former is that the grain shape experiences the same change as the whole body of material and the relative location of adjacent grains stays almost unchanged. The feature of the latter is that the grains do not change themselves and the relative location of adjacent grains changes. At high temperatures of 450 °C (0.77T_m, where T_m is the melting point of aluminum), the deformation process is inclined to achieve by the GB sliding, but the possibility of the GB sliding in Composites I, II and III was supressed because of the strong pinning effect of lamellar Al_2O_3 located at the GBs [10]. Thus, the deformation would be more dependent on quasi-uniform flow by deformation of the grains, which could cause flattening of Al grains.

As for Composite IV, the pinning effect of γ-Al_2O_3 on the GB gliding was much weaker [19], hence, the GB gliding contributed more to the deformation process. Thus, the shape change of Al grains was slighter. Another macroscopical phenomenon that could further confirm this speculation is that the distribution of the B_4C particles in Composite IV was more uniform than that in Composites II and III (Fig. 2). It is because in the quasi-uniform flow in Composites II and III, the change of the relative location of the grains was less, so the B_4C particles could hardly change their locations with the matrix flow and the uneven distribution of B_4C particles was preserved. On the contrary, the B_4C in Composite IV was dispersed uniformly in the matrix with the Al grains changing their relative location, so the distribution of B_4C was much more uniform.

In a hot deformation process, it was reported that the sub-grain size (λ) exhibited an inverse variation with stress [23,24],

$$\lambda / b = 23(G / \sigma) \quad (1)$$

where G is the shear modulus and σ is the flow stress. By calculating with this formula, a λ of 1 μm corresponds to the σ of 151 MPa. According to the tensile tests, the flow stress in the present study was much lower than

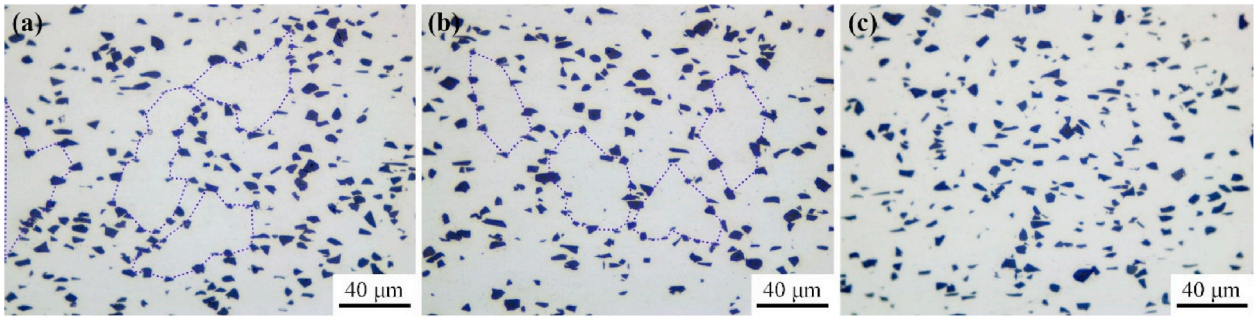

Fig. 2. Optical micrographs showing the distribution of B_4C particles in (a) Composite II, (b) Composite III and (c) Composite IV.

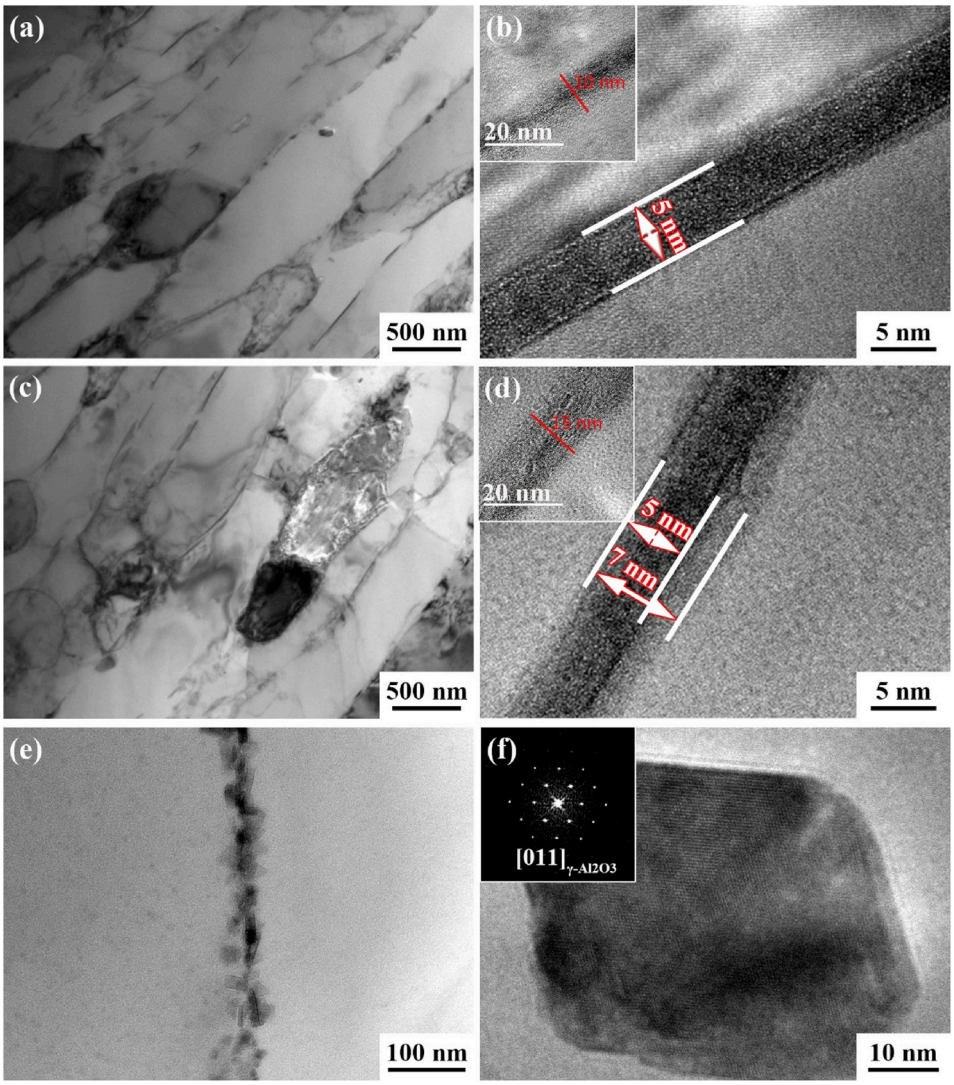

Fig. 3. TEM micrographs showing the distribution of Al_2O_3 in (a) Composite II, (c) Composite III, and (e) Composite IV; higher-magnification TEM micrographs showing the Al_2O_3 in (b) Composite II, (d) Composite III, and (f) Composite IV.

151 MPa. Therefore, the λ decided by flow stress in this study should be much larger than 1 μm, which was larger than the actual grain size. In this situation, the Al_2O_3 spacing is smaller than the size predicted by the stress-dependent substructure, so the grain (or sub-grain) size was governed by Al_2O_3 spacing [24]. Therefore, only a little sub-grain boundaries were observed in these composites.

3.2. Mechanical properties

The engineering stress–strain curves of the four composites at RT are shown in Fig. 5a and the tensile properties are listed in Table 2. Composites I, II, III and IV all showed higher strength than conventional B_4C/Al composite (Composite V). Compared to Composite I, the yield strength (YS) and ultimate tensile strength (UTS) of Composite II increased by 4.7 MPa and 10.9 MPa, respectively, due to the addition of 10.0 wt% B_4C particles. After increasing Al_2O_3 content by pre-oxidation, the YS and UTS of composite III further increased by 7.9 MPa and 11.6 MPa. For Composite IV which experienced higher HIP temperature of 550 °C, the strength decreased significantly because am-Al_2O_3 transformed into γ-Al_2O_3, which was reported in Ref. [19]. This confirmed the more prominent strengthening effect of am-Al_2O_3 than γ-Al_2O_3. Meanwhile, Composite IV exhibited almost the same elongation as Composite I despite its much lower strength. This indicates that the nano-scale lamellar Al_2O_3 could strengthen the composite to higher strength without causing excessive ductility loss.

Results of tensile tests at 350 °C are shown in Fig. 5b and listed in Table 3. The mechanical properties at 350 °C were quite different from those at RT. For Composites I, II and III, the YS and UTS exhibited almost the same values at 350 °C. That is to say, neither adding B_4C particles nor increasing the Al_2O_3 content could increase the composite strength at 350 °C. This implies that the strengthening mechanism at 350 °C was quite different from that at RT and the load-transfer effect became insignificant.

At 350 °C, elongation was still reduced by the addition of the reinforcements, indicating the impaired deformation ability, which could be caused by inconsistent deformation at the interfaces. Obvious decrease in tensile ductility of Composites I, II and III at elevated temperatures was consistent with other studies [10,19]. This phenomenon can be explained by dislocation annihilation at the grain boundaries. At high temperature, the dislocations were annihilated by dynamic recovery, resulting in the lack of work hardening; on the other hand, the GB gliding was hindered by am-Al_2O_3, so elongation exhibited lower values at 350 °C.

The crystallization of am-Al_2O_3 decreased the tensile strength at 350 °C significantly. Compared with the tensile results at RT, the strengthening effect of am-Al_2O_3 was proven to be more significant at high

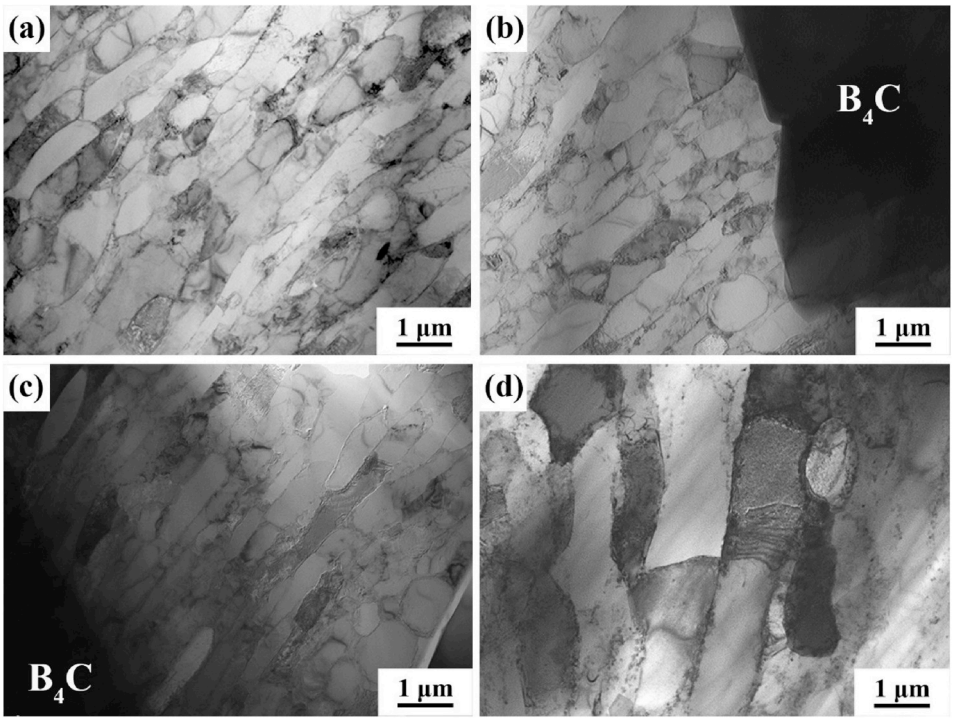

Fig. 4. TEM micrographs showing the grain structure in (a) Composite I, (b) Composite II, (c) Composite III and (d) Composite IV.

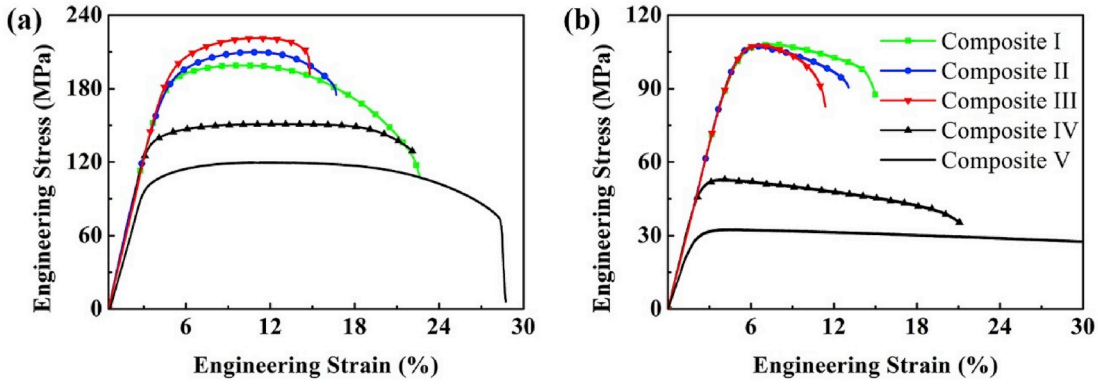

Fig. 5. Engineering stress–strain curves of the composites at (a) RT and (b) 350 °C.

Table 2
Tensile properties of the composites at RT.

Sample	YS (MPa)	UTS (MPa)	El (%)
Composite I	154.6 ± 4.6	198.9 ± 2.2	20.5 ± 2.3
Composite II	159.3 ± 5.1	209.8 ± 1.9	13.3 ± 1.6
Composite III	167.2 ± 5.1	221.4 ± 1.8	10.7 ± 3.3
Composite IV	122.2 ± 3.6	147.9 ± 0.8	19.4 ± 3.6
Composite V	91.8 ± 6.1	120.6 ± 1.2	26.4 ± 3.6

Table 3
Tensile properties of the composites at 350 °C.

Sample	YS (MPa)	UTS (MPa)	El (%)
Composite I	93.8 ± 3.1	108.9 ± 2.7	12.3 ± 3.2
Composite II	95.2 ± 2.2	106.2 ± 2.2	9.6 ± 2.7
Composite III	94.8 ± 4.2	107.6 ± 3.1	7.6 ± 3.2
Composite IV	42.6 ± 2.2	53.0 ± 1.2	19.8 ± 3.4
Composite V	26.4 ± 2.4	33.6 ± 2.3	55 ± 5.2

temperature, because the YS of Composite IV at 350 °C was less than half of that of Composites I, II and III. It can be concluded that the lamellar am-Al_2O_3 was more crucial in enhancing high-temperature strength. Also, all composites fabricated using ultrafine Al powders showed higher strength than conventional B_4C/Al composite (Composite V).

4. Discussion

4.1. Deformation mechanism at 350 °C

Fig. 6a shows the true stress–strain curves of Composites II and IV at 350 °C with different initial strain rates. For both composites, the flow stress increased with the increase of strain rate. As for elongation, both materials exhibited an increasing elongation as strain rate increased from 10^{-4} to 10^{-2} s^{-1}. However, when strain rate increased to 10^{-1} s^{-1}, a decreased elongation was observed. The similar tendency of the two composites in the deformation behaviour indicates that the deformation mechanism may be similar in spite of different strength values.

Previous studies revealed that at low strain rates, dynamic recovery

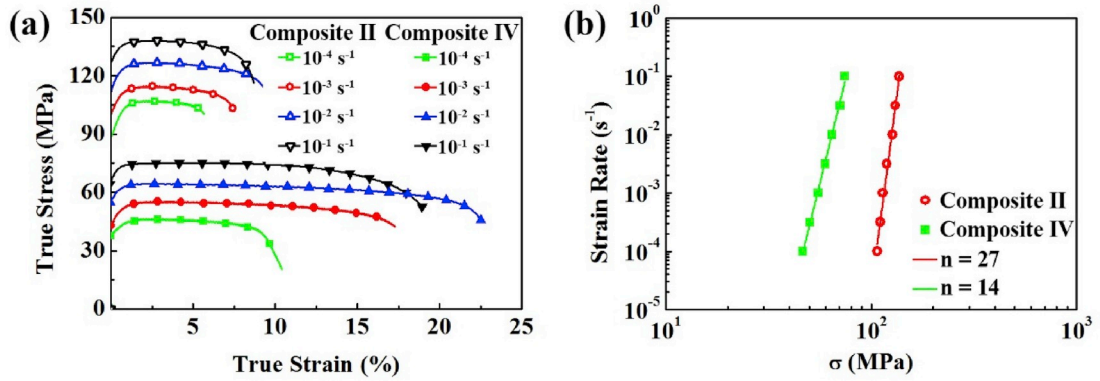

Fig. 6. (a) Tensile true stress–strain curves of composites II and IV, and (b) initial strain rate against maximum stress curves on a double log scale.

was more dominant and dislocations interacted with Al_2O_3 at the GBs, which could lead to localized plastic deformation and promote void formation, thus, with the increase of the strain rate, less recovery happened and ductility was increased [10,25]. When strain rate increased to a higher value as 10^{-1} s^{-1}, there was not enough time for diffusion to restore the defects, resulting in decreased elongation.

Fig. 6b shows the variation of strain rate with flow stress at the peak point on double logarithmic coordinate. A linear relationship was shown and high apparent stress exponents of 27 and 14 were obtained for Composites II and IV, respectively. High values of apparent stress exponents were often reported in particle reinforced AMCs [26–28], which could be interpreted by the concept of effective stress, $\sigma^{*} = \sigma - \sigma_{th}$, where σ is applied stress and σ_{th} is threshold stress [24,29].

For the AMCs, the deformation mechanisms are usually associated with lattice diffusion controlled dislocation-climbing creep (n = 5), pipe diffusion controlled dislocation-climbing creep (n = 7) and lattice diffusion controlled invariant substructure creep (n = 8), where n is the stress exponent [24,27]. As shown in Fig. 7, the n and σ_{th} were determined using the linear regression method by assuming the stress exponent (5, 7 and 8) first [27,28]. The best result was decided by the largest R^2. For both Composites II and IV (Fig. 7a), the best linear fit was achieved when n = 8 was used, indicating that although the strength values were quite different, the main deformation mechanism of two composites is the same lattice diffusion controlled substructure-invariant.

A principal equation generalizing dislocation creep (governed by lattice diffusion) was proposed by Sherby [30,31]:

$$\dot{\varepsilon} = B\frac{D_L}{b^2}(\lambda/b)^3(\sigma/E)^8 \quad (2)$$

where B is the constant depending on stacking fault energy, λ is the minimum barrier spacing or sub-grain size, b is the Burgers vector, σ is the flow stress, E is the Young's modulus of matrix and D_L is the lattice diffusion coefficient.

For most traditional materials such as metallic alloys, λ is strongly dependent on σ, and Sherby first proposed the basic relation of σλ = constant [32]. Thus, Eq. (2) reduces to the five power law equation and the value of n ($= \partial ln\dot{\varepsilon}/\partial ln\sigma$) could be obtained as 5, representing the mechanism of dislocation climb (lattice diffusion). However, for some AMCs, λ is decided by the interparticle spacing (λ = constant) [27,33], so the n under dislocation climb (lattice diffusion) mechanism with a constant structure could be obtained as 8.

The similarity in the deformation mechanism of Composites II and IV can be rationalized by the precondition of substructure-invariant [27]. According to Eq. (1), the stress range in the present study would result in larger sub-grain size than the actual grain size. The am-Al_2O_3/γ-Al_2O_3 at the GBs could prevent the growth of the grains strongly [20], so the interparticle spacing instead of the applied stress decided the size of the grains (λ = constant). Thus, the deformation of the composites at 350 °C can be described by the "constant structure" model over stress range used in this study.

In some studies, it was considered that when deformation was associated with the substructure-invariant mechanism, in which the sub-grains are stable in size, large increase in strength could be resulted [24,31]. However, the sameness in the deformation mechanism and the discrepancy in high-temperature stress of Composites II and IV indicated that the deformation mechanism was not the reason for the disparity in the strength of Composites II and IV. Therefore, it is necessary to discuss the strengthening mechanisms of the composites further to illuminate the enhanced strength.

The threshold stresses of Composites II and IV at 350 °C were 84.7 and 26.5 MPa. Although the origin of σ_{th} remains controversial, higher σ_{th} indicates a stronger resistance to deformation.

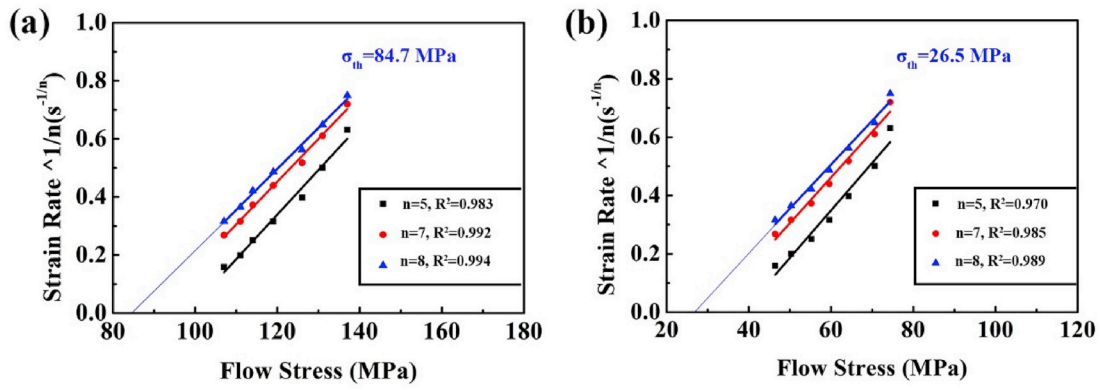

Fig. 7. Determination of σ_{th} for (a) Composite II and (b) Composite IV.

4.2. Strengthening mechanisms at 350 °C

At 350 °C, Composites I and II exhibited nearly the same strength, so the strengthening effect of B_4C particles was proven to vanish at such a high temperature, which was consistent with Ref. [27]. One possible reason for this phenomenon was that load-transfer strengthening was restricted by relaxation process of dislocations and stress field, which was caused by diffusional assisted flow [34]. On the other hand, the interparticle spacing of B_4C was too large to exert effects on a microscopic scale. Therefore, the strengthening effect of B_4C was insignificant at high temperatures.

For the lamellar am-Al_2O_3, there are two main strengthening effects which should be considered when analyzing the strength discrepancy of the composites in the present study: 1) load-transfer effect which is more vital for lamellar reinforcements [35] and 2) strengthening effect by pinning GBs which was confirmed in the Al_2O_3/Al composites by previous study [10].

1) Load-transfer effect

For load-transfer effect of lamellar Al_2O_3, the modified shear lag model proposed by Nardone [35] can be taken into consideration. The yield strength contributed by platelets can be expressed as:

$$\sigma_c = \sigma_m \left[\frac{V_P(S+4)}{4} + V_m \right] \tag{3}$$

where σ_c is the composite strength, σ_m is the strength of Al matrix, V_P is the content of Al_2O_3, V_m is the content of Al matrix and S is the ratio of the length to thickness of the platelet. According to this model, the strengthening factor of am-Al_2O_3 in Composites II and III was only 1.27 and 1.32, respectively. By comparing with the YS at 350 °C of Composites IV or V, it was found that the significant increase in the YS of Composites II and III cannot be explained by the load-transfer effect. Furthermore, if the load-transfer strengthening effect can still play an important role at 350 °C, the YS of Composite III would be ~4% higher than that of Composite II, just like the situation at RT. Clearly, the same YS of Composites II and III also indicated the invalidation of load-transfer strengthening of Al_2O_3 at 350 °C.

2) Strengthening effect by pinning GBs

By comparing Composites II and IV, the strengthening effect of lamellar am-Al_2O_3 was highlighted. In the discussion of deformation mechanism, it has been revealed that these two composites were both deformed under the same substructure-invariant mechanism. Fig. 8a and b shows grain microstructure of Composites II and IV after tensile testing at 350 °C, respectively. It was revealed that the grain size of both composites did not exhibit obvious variation, which was in accordance with the substructure-invariant mechanism discussed above.

By analyzing Eqs. (1) and (2), it could be seen that the essence of substructure-invariant mechanism is that the interparticle spacing in the composites is smaller than the sub-grain size predicted by the λ-σ relation, and the sub-grain/grain size does not change with the flow stress [27]. However, at such a high temperature of 350 °C (0.66 T_m), the GB gliding was easy to happen, which was to the disadvantage of high-temperature strength. Therefore, the pinning effect of Al_2O_3 which could prevent the GBs from gliding was much more important at high temperature.

In Fig. 8a, the dark contrast near the GBs indicated dislocation accumulation, the reason for which could be that the GB gliding was hindered by lamellar am-Al_2O_3, as reported in Ref. [36]. The marked difference in Composite IV (Fig. 8b) was that the Al grains were almost free of dislocations and clean GBs were disclosed. Particulate γ-Al_2O_3 could not pin the GBs effectively, therefore, the GB gliding could be easier. It was reported that the GB gliding required accommodation of dislocation annihilation [37]. Consequently, the GB gliding and dislocation annihilation at the GBs in Composite IV resulted in much lower strength. That is to say, the large disparity in the strength of Composites II and IV was caused by different GB pinning effect of am-Al_2O_3 lamellae and γ-Al_2O_3 particles. Furthermore, the same strength of Composites II and III indicated that increasing the thickness of Al_2O_3 film could not increase its pinning effect on the GBs and therefore could not contribute to enhance the high-temperature strength.

By observation of fracture surfaces of Composites II and IV, it could further confirm that the difference in strength at 350 °C arose from the GB gliding. Fig. 9 shows the SEM fractographes of Composites II and IV at RT and 350 °C at a strain rate of 1×10^{-3} s^{-1}. At RT, ductile fracture could be seen and the dimples in Composite IV (Fig. 9b) were larger and deeper than those in Composite II (Fig. 9a). At 350 °C, both composites showed intergranular fracture and nearly no dimples could be seen.

As reported in Ref. [10], the recovery behavior at the GBs could lead to localized deformation and provoke voids and fracture, resulting in intergranular fracture at high temperature. It can be seen on the fracture surface of Composite IV (Fig. 9d) that obvious relative gliding happened among the contiguous grains, resulting in evident gaps (white arrows). More notably, the fractograph even exhibited a similar morphology to that in some super-plastic AMCs in which the GB gliding mechanism mainly dominated the deformation process [38], indicating that the GB gliding happened in the deformation and fracture of Composite IV. As for Composite II (Fig. 9c), since the GB gliding was suppressed by am-Al_2O_3, less GB gliding happened and a flatter fractograph was seen.

5. Conclusions

In this study, (B_4C + Al_2O_3)/Al composites were fabricated using ultrafine Al powders as the neutron absorbing materials (NAMs) for structural usages. The enhanced strength was studied with both deformation mechanisms and strengthening mechanisms being taken into

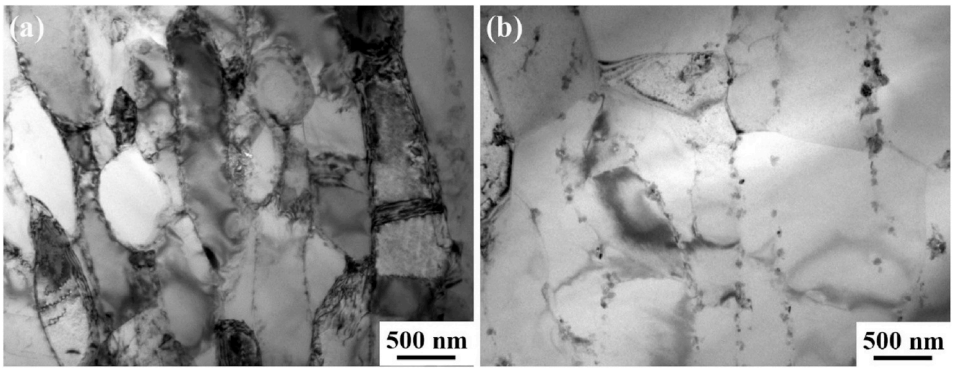

Fig. 8. TEM images showing grain microstructure in Composites (a) II and (b) IV after tensile testing at 350 °C.

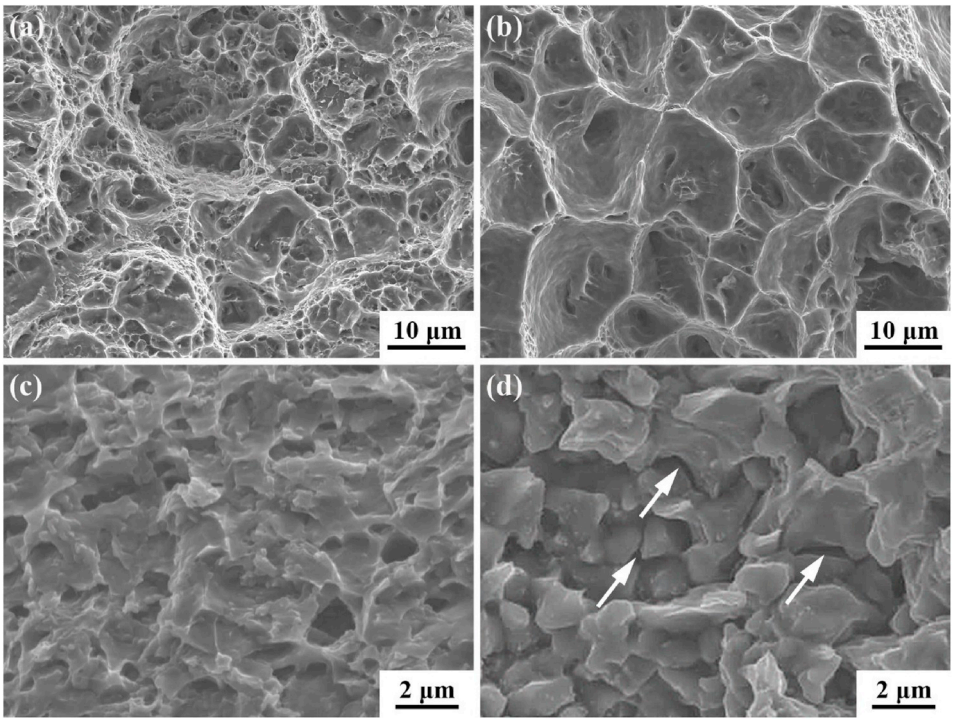

Fig. 9. SEM fractographs of Composite II at (a) RT and (c) 350 °C; and of Composite IV at (b) RT and (d) 350 °C.

consideration. The following conclusions are made:

1. The ($B_4C + Al_2O_3$)/Al NAMs were successfully produced with HIP at 450 °C, in which the lamellar am-Al_2O_3 was remained. The ultimate tensile strength was 106.2 MPa and the elongation was 9.6% at 350 °C. However, when HIP was performed at 550 °C, lamellar am-Al_2O_3 was transformed into γ-Al_2O_3 particles, which led to serious deterioration of the strength.
2. The addition of B_4C particles and the increase in the thickness of am-Al_2O_3 film could both increase the composite strength at RT. However, at 350 °C, they could not increase the strength because of the invalidation of the load-transfer strengthening effect.
3. Despite the large discrepancy in strength (as high as 100%), the deformation of the composites reinforced by am-Al_2O_3 and γ-Al_2O_3 was both dominated by the lattice diffusion controlled substructure-invariant mechanism at 350 °C.
4. The better high-temperature strength of the composite containing am-Al_2O_3 was attributed to the pinning effect of lamellar Al_2O_3 against the GB gliding.

Declaration of competing interest

The author declares that they have no known competing financial interests or personal relationships that could have appeared to influence the work reported in this paper.

Acknowledgements

The authors gratefully acknowledge the support of (a) the National Natural Science Foundation of China under grant Nos. U1508216 and 51771194, (b) the Youth Innovation Promotion Association CAS (2016179), and (c) the National Key R & D Program of China (No. 2017YFB0703104).

Appendix A. Supplementary data

Supplementary data to this article can be found online at https://doi.org/10.1016/j.msea.2019.138840.

Author contribution statement

Y.N. Zan: Methodology, Investigation, Visualization, Writing – original draft. **Y.T. Zhou**: Investigation, Visualization, Writing – original draft. **Z.Y. Liu**: Formal analysis. **Q.Z. Wang**: Project administration, Funding acquisition. **W.G. Wang**: Resources, Data curation. **D. Wang**: Resources. **B.L. Xiao**: Conceptualization, Writing - review & editing, Funding acquisition. **Z.Y. Ma**: Supervision, Writing - review & editing, Funding acquisition.

Data Availability

The raw/processed data will be made available on request.

References

[1] H.S. Chen, W.X. Wang, Y.L. Li, P. Zhang, H.H. Nie, Q.C. Wu, The design, microstructure and tensile properties of B_4C particulate reinforced 6061Al neutron absorber composites, J. Alloy. Comp. 632 (2015) 23–29.
[2] H.S. Chen, W.X. Wang, Y.L. Li, J. Zhou, H.H. Nie, Q.C. Wu, The design, microstructure and mechanical properties of B_4C/6061Al neutron absorber composites fabricated by SPS, Mater. Des. 94 (2016) 360–367.
[3] Y.T. Zhou, Y.N. Zan, S.J. Zheng, X.H. Shao, Q.Q. Jin, B. Zhang, X.L. Ma, B.L. Xiao, Q.Z. Wang, Z.Y. Ma, Thermally stable microstructures and mechanical properties of B_4C-Al composite with in-situ formed Mg(Al)B_2, J. Mater. Sci. Technol. 35 (2019) 1825–1830.
[4] X. Pang, Y. Xian, W. Wang, P. Zhang, Tensile properties and strengthening effects of 6061Al/12 wt%B_4C composites reinforced with nano-Al_2O_3 particles, J. Alloy. Comp. 768 (2018) 476–484.
[5] H.S. Chen, W.X. Wang, H.H. Nie, J. Zhou, Y.L. Li, R.F. Liu, Y.Y. Zhang, P. Zhang, Microstructure evolution and mechanical properties of B_4C/6061Al neutron absorber composite sheets fabricated by powder metallurgy, J. Alloy. Comp. 730 (2018) 342–351.
[6] Y.Z. Li, Q.Z. Wang, W.G. Wang, B.L. Xiao, Z.Y. Ma, Interfacial reaction mechanism between matrix and reinforcement in B_4C/6061Al composites, Mater. Chem. Phys. 154 (2015) 107–117.
[7] Y.Z. Li, Q.Z. Wang, W.G. Wang, B.L. Xiao, Z.Y. Ma, Effect of interfacial reaction on age-hardening ability of B_4C/6061Al composites, Mater. Sci. Eng. A 620 (2015) 445–453.

[8] J. Qin, Z. Zhang, X.G. Chen, Mechanical properties and strengthening mechanisms of Al-15 Pct B_4C composites with Sc and Zr at elevated temperatures, Metall. Mater. Trans. A 47 (2016) 4694–4708.
[9] Z.G. Xu, L.T. Jiang, Q. Zhang, J. Qiao, L.C. Zhang, P. He, J. Ma, G.H. Wu, The formation, evolution and influence of Gd-Containing phases in the (Gd+B_4C)/6061Al composites during hot rolling, J. Alloy. Comp. 775 (2019) 714–725.
[10] C. Poletti, M. Balog, F. Simancik, H.P. Degischer, High-temperature strength of compacted sub-micrometer aluminium powder, Acta Mater. 58 (2010) 3781–3789.
[11] A. Morri, L. Ceschini, S. Messieri, E. Cerri, S. Toschi, Mo Addition to the A354 (Al-Si-Cu-Mg) Casting Alloy: Effects on Microstructure and Mechanical Properties at Room and High Temperature, Metals, 2018, p. 8.
[12] G.J. Li, H.C. Liao, X.J. Suo, Y.Y. Tang, U.S. Dixit, P. Petrov, Cr-induced morphology change of primary Mn-rich phase in Al-Si-Cu-Mn heat resistant aluminum alloys and its contribution to high temperature strength, Mater. Sci. Eng. A 709 (2018) 90–96.
[13] X.H. Wang, Z.Y. Liu, S. Bai, L.H. Lin, C.W. Ye, H. Wang, Enhanced heat resistance of Al-Cu-Mg alloy by a combination of pre-stretching and underaging, J. Mater. Eng. Perform. 25 (2016) 3793–3801.
[14] D.H. Xiao, J.N. Wang, D.Y. Ding, S.P. Chen, Effect of Cu content on the mechanical properties of an Al–Cu–Mg–Ag alloy, J. Alloy. Comp. 343 (2002) 77–81.
[15] D.H. Xiao, J.N. Wang, D.Y. Ding, H.L. Yang, Effect of rare earth Ce addition on the microstructure and mechanical properties of an Al–Cu–Mg–Ag alloy, J. Alloy. Comp. 352 (2003) 84–88.
[16] J.S. Benjamin, M.J. Bomford, Dispersion strengthened aluminum made by mechanical alloying, Metall. Trans. A 8 (1977) 1301–1305.
[17] E.A. Bloch, Dispersion-strengthened aluminium alloys, Metall. Rev. 6 (1961) 193–240.
[18] Z. Li, Q. Guo, Z.Q. Li, G.L. Fan, D.B. Xiong, Y.S. Su, J. Zhang, D. Zhang, Enhanced mechanical properties of graphene (reduced graphene oxide)/aluminum composites with a bioinspired nanolaminated structure, Nano Lett. 15 (2015) 8077–8083.
[19] M. Balog, C. Poletti, F. Simancik, M. Walcher, W. Rajner, The effect of native Al_2O_3 skin disruption on properties of fine Al powder compacts, J. Alloy. Comp. 509 (2011) S235–S238.
[20] M. Balog, P. Krizik, M. Nosko, Z. Hajovska, M. Victoria Castro Riglos, W. Rajner, D.-S. Liu, F. Simancik, Forged HITEMAL: Al-based MMCs strengthened with nanometric thick Al_2O_3 skeleton, Mater. Sci. Eng., A 613 (2014) 82–90.
[21] S.E. Shin, H.J. Choi, J.H. Shin, D.H. Bae, Strengthening behavior of few-layered graphene/aluminum composites, Carbon 82 (2015) 143–151.
[22] M.F. Ashby, R.A. Verrall, Diffusion-accommodated flow and superplasticity, Acta Metall. 21 (1973) 149–163.
[23] S.V. Raj, G.M. Pharr, A compilation and analysis of data for the stress dependence of the subgrain size, Mater. Sci. Eng. 81 (1986) 217–237.
[24] W. Kim, S.H. Lee, High-temperature deformation behavior of carbon nanotube (CNT)-reinforced aluminum composites and prediction of their high-temperature strength, Compos. Part A 67 (2014) 308–315.
[25] S.-S. Kim, M.J. Haynes, R.P. Gangloff, Localized deformation and elevated-temperature fracture of submicron-grain aluminum with dispersoids, Mater. Sci. Eng. A 203 (1995) 256–271.
[26] Z.Y. Ma, S.C. Tjong, Y.L. Li, Y. Liang, High temperature creep behavior of nanometric Si_3N_4 particulate reinforced aluminium composite, Mater. Sci. Eng. A 225 (1997) 125–134.
[27] S.H. Wang, P.W. Kao, The strengthening effect of Al_3Ti in high temperature deformation of Al-Al_3Ti composites, Acta Mater. 46 (1998) 2675–2682.
[28] Z.Y. Ma, S.C. Tjong, Creep deformation characteristics of discontinuously reinforced aluminium-matrix composites, Compos. Sci. Technol. 61 (2001) 771–786.
[29] S.C. Tjong, Z.Y. Ma, The high-temperature creep behaviour of aluminium-matrix composites reinforced with SiC, Al_2O_3 and TiB_2 particles, Compos. Sci. Technol. 57 (1997) 697–702.
[30] O.D. Sherby, J. Wadsworth, Superplasticity—recent advances and future directions, Prog. Mater. Sci. 33 (1989) 169–221.
[31] O.D. Sherby, R.H. Klundt, A.K. Miller, Flow stress, subgrain size, and subgrain stability at elevated temperature, Metall. Trans. A 8 (1977) 843–850.
[32] O.D. Sherby, P.M. Burke, Mechanical behavior of crystalline solids at elevated temperature, Prog. Mater. Sci. 13 (1968) 323–390.
[33] Z.Y. Ma, J. Bi, Y.X. Lu, Tensile creep behaviour of silicon carbide particulate reinforced aluminium composite, J. Mater. Sci. Technol. 14 (1998) 33–36.
[34] J. Rösler, G. Bao, A.G. Evans, The effects of diffusional relaxation on the creep strength of composites, Acta Metall. Mater. 39 (1991) 2733–2738.
[35] V.C. Nardone, K.M. Prewo, On the strength of discontinuous silicon carbide reinforced aluminum composites, Scr. Metall. 20 (1986) 43–48.
[36] Y.N. Zan, Y.T. Zhou, H. Zhao, Z.Y. Liu, Q.Z. Wang, D. Wang, W.G. Wang, B.L. Xiao, Z.Y. Ma, Enhancing high-temperature strength of (B_4C+Al_2O_3)/Al designed for neutron absorbing materials by constructing lamellar structure, Compos. Part B 183 (2020) 107674.
[37] Y. Qi, P.E. Krajewski, Molecular dynamics simulations of grain boundary sliding: the effect of stress and boundary misorientation, Acta Mater. 55 (2007) 1555–1563.
[38] G.L. Fan, H.Y. Huang, Z.Q. Tan, D.B. Xiong, Q. Guo, M. Naito, Z.Q. Li, D. Zhang, Grain refinement and superplastic behavior of carbon nanotube reinforced aluminum alloy composite processed by cold rolling, Mater. Sci. Eng. A 708 (2017) 537–543.